J Mater Sci (2024) 59:8040–8057

Polymers & biopolymers

Development of binary and ternary polyester shape memory blends for additive manufacturing

Luis E. Lares Carrillo[1,3], Yareli O. Gonzalez[1,3], Marilyn Parga[1,3], Katia Lizbeth Delgado Ramos[1,3], Nadya Neparko[2], and David A. Roberson[1,3,*]

[1] *Polymer Extrusion Lab, The University of Texas at El Paso, El Paso, TX, USA*
[2] *Desert Learning Academy, Vado, NM, USA*
[3] *Department of Metallurgical, Materials and Biomedical Engineering, The University of Texas at El Paso, El Paso, TX, USA*

Received: 26 November 2023
Accepted: 7 April 2024
Published online: 26 April 2024

ABSTRACT

The goal of this work was to create shape memory polymer blends for the additive manufacturing technology of fused filament fabrication. An iterative approach was taken to develop a binary blend of polycaprolactone (PCL) and thermoplastic urethane (TPU). The composition of equal parts by mass PCL and TPU exhibited the best mechanical and shape memory properties. It was then decided to compound a ternary blend of PCL, TPU, and polylactic acid (PLA) where all components were of equal parts by mass. Constituents were chosen because they are all long chain polyesters with similar Hildebrand solubility parameters, because they are biocompatible, and because they all have some level of shape memory properties on their own. Dynamic mechanical analysis was performed to determine the recovery temperature for specimens that were deformed at room temperature. Scanning electron microscopy was used to perform fracture surface analysis of spent tensile test specimens. X-ray diffraction was used to explore aspects related to crystallinity of the blend materials. Transmission electron microscopy was used to characterize the mixing of the blend constituents where both the binary and ternary blends were found to be immiscible. The work presented here demonstrates materials selection based on structure, polymer family, and solubility parameter as a strategy for the development of multi-constituent polymer blends without the use of compatibilizers.

Introduction

Shape memory polymers (SMPs) can be deformed into a temporary shape and then recover their original shape after a stimulus is applied. This stimulus could be heat, force, electromagnetic radiation, or moisture, among others [1]. In the case of heat-activated SMPs, a temporary shape can be obtained when the specimen is deformed at a temperature at or below the material's glass transition temperature (T_g) and then recovered

Handling Editor: Jaime Grunlan.

Address correspondence to E-mail: droberson@utep.edu

https://doi.org/10.1007/s10853-024-09657-7

by heating the specimen above the T_g [2]. Interest in shape memory polymers has steadily increased, and this class of plastics has been used in applications ranging from wound sutures to aerospace components [3, 4]. When SMPs are combined with additive manufacturing (AM), also referred to as 3D printing, the terminology "4D printing" is sometimes used [2, 5]. An example of the shape memory process for an object fabricated by AM using a ternary blend characterized in this study is shown in Fig. 1.

Shape memory properties can be quantified by calculating two critical parameters: (1) the fixation ratio (R_f), the ability of a material to hold a temporary shape; and (2) the shape recovery ratio (R_r), the ability of a material to return to the permanent or "programmed" shape. These parameters are determined by the following equations [2, 5–8],

$$R_f(\%) = \frac{\varepsilon_u}{\varepsilon_m} \times 100\% \quad (1)$$

$$R_r(\%) = \frac{\varepsilon_m - \varepsilon_p}{\varepsilon_m} \times 100\% \quad (2)$$

where ε_m is the maximum strain applied to a test specimen, which is generally 100% elongation, ε_u is the elongation of the specimen after removal of applied load, and ε_p is the elongation of the specimen application of a recovery process. The shape memory index (SMI) can then be calculated by multiplying R_r by R_f (Eq. 3) and is useful for discriminating the difference between a rubber and a true shape memory polymer [2, 9].

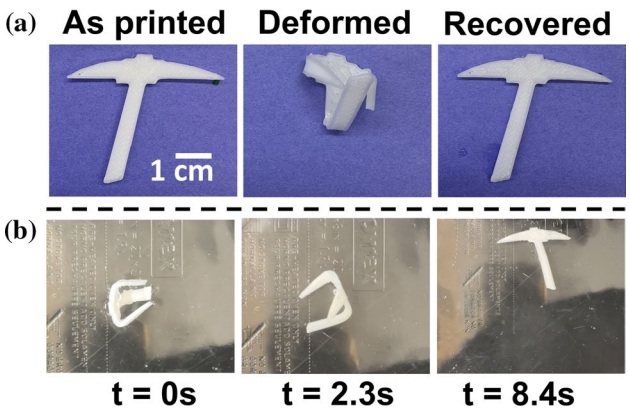

Figure 1 **a** Shape memory cycle for an object made by FFF from the ternary blend used in this study where the as printed state is the programmed shape. **b** Time-lapse of a deformed object being recovered in water at a temperature of 65 °C.

$$\mathrm{SMI}(\%) = (R_r \times R_f) \times 100\% \quad (3)$$

The work presented here explores binary shape memory polymer blends composed of polycaprolactone (PCL) and thermoplastic urethane (TPU) and a ternary blend composed of PCL, TPU, and polylactic acid (PLA). On their own PCL and TPU both have shape memory properties [5, 10, 11] and examples in the literature demonstrate a relatively broad use of blends composed of these two constituents. For example, work performed by Jing et al. [12] demonstrated the manufacture of self-knotting structures from a blend of PCL and TPU. Polymer matrix composites where the matrix material is a blend composed of PCL and TPU have also been demonstrated in the literature with various filler materials. For example, Xu et al. [13] combined a blend of PCL and TPU with multi-wall carbon nanotubes (MWCNT)s and showed that the addition of MWCNTs allowed shape memory and self-healing functionality upon the exposure to ultraviolet light where this was not found to be the case for the matrix material alone.

PLA is a plant-derived, biodegradable polymer [14, 15] and has a broad spectrum of applications including food packaging, 3D printer feedstock, and biomedical uses [1, 6, 16–19]. As is the case with PCL and TPU, PLA has robust shape memory properties on its own. Combining PLA with PCL was shown to be beneficial in biomedical applications as it was noted by Ebrahimi et al. [20] that the acidity of PLA was reduced by the addition of PCL, thereby reducing the inflammatory response when used in tissue engineering. Furthermore, blending PLA with TPU has been shown to yield polymer blends with good shape memory characteristics [5, 9]. Though there are many examples for the creation of both PCL/TPU and PLA/TPU shape memory polymer blends [12, 21–23], there is not a large body of work that explores ternary thermoplastic blends composed of PLA, PCL, and TPU so we believe the findings in this study to be novel.

Our group has demonstrated the development of binary and ternary blends for FFF in a previous work involving acrylonitrile butadiene styrene (ABS), styrene ethylene butylene styrene (SEBS), and ultra-high molecular weight polyethylene (UHMWPE) [24], where the strategy was similar to that of traditional metal alloying in that the basis was ABS and the other constituents were added in incremental amounts. In the work presented here, we follow a design strategy for shape memory polymer blends

that our group first presented in works by Quiñonez et al. [5, 25] where we relied upon similarities in polymer characteristics to facilitate blending, where one of the blends studied was composed of PLA and TPU. First, we present an iterative process for the development of a PCL/TPU blend where a 50/50 by mass ratio composition proved to be the most compatible with the AM process of fused filament fabrication (FFF). PLA was then added creating a ternary blend where the constituents were in equal parts by mass.

One materials selection criterion for the constituents used in this study was the Hildebrand solubility parameter (δ). For PLA, δ ranges between 19.9 and 20.7 $MPa^{1/2}$ [26], while the δ for PCL varies from 15.8 to 21.2 $MPa^{1/2}$ [27] and the δ for TPU is in the order of 20 $MPa^{1/2}$ [28]. An additional criterion used to select the materials evaluated in this study was the fact that all three constituents are biocompatible and we wish to ascertain the use of these material systems in biomedical applications in future efforts. In addition to similar solubility parameters, all three materials studied in this work are long chain linear polyesters and, as mentioned above, all have inherent shape memory polymers. In short, all constituents in the blends evaluated here were chosen due to their similar solubility parameters, all belonging to the same polymer family, biocompatibility, and the possession of shape memory properties. Also, the combination of TPU, an elastomer, with PLA and/or PCL allows for room temperature deformation of the resultant blends. The effort presented here is part of a larger body of work by Lares Carillo [29] and demonstrates a facile materials design approach that can facilitate the development of multi-constituent polymer blends for AM without the need for compatibilizers of solvents. We believe that the presented approach could also be used to create high entropy polymer blends where the total number of constituents is five.

Materials and methods

Initial experiments focused on the development of a binary blend composed of PCL and TPU where the ratio of each constituent was varied in discrete amounts by mass (75% PCL 25% TPU, 50% PCL 50% TPU, 25% PCL 75% TPU). We chose to compound the ternary blend following the strategy of a high entropy material and only created an iteration of equal parts (by mass) of PLA, PCL, and TPU. The binary and ternary polymer blends were produced through the process of melt compounding using a Collin twin-screw extruder/compounder (Model ZK 25-T, Collin Lab and Pilot Solutions, Norcross, GA, USA) equipped with a melt pump and belt puller. Filaments were extruded with a target diameter of 2.85 mm to be compatible with the FFF machine used in this study. The extrusion parameters for the blends evaluated hare are listed in Table 1.

The PLA used in this work was obtained from NatureWorks, LLC (Ingeo Biopolymer Grade 4043D, NatureWorks, LLC, Minnetonka MN, USA) in pellet form. The TPU used in this work was obtained from NinjaTek (NinjaFlex, Fenner Precision Polymers, Lititz, PA, USA) and was received in filament form which was later pelletized using a Collin strand pelletizer (Model SP1 Collin Lab and Pilot Solutions, Norcross, GA, USA). The PCL used in this work was obtained from Polly Plastics (Midland, MI, USA) and was received in pellet form. Prior to processing, the PLA was dried for 2 h at 50 °C using a compressed air dryer (Micro Dryer CAFM station, Dri-Air Industries, East Windsor, CT, USA). The temperature parameters for the extrusion of PCL and TPU blends were determined based on previous studies found in literature [12, 30, 31]. Different cooling methods were needed since the stickiness of the PCL made it difficult to extrude and spool. As such, the blend iteration with the highest PCL content (75% PCL/25%TPU) required water cooling of the extruded filament prior to spooling. The extrusion parameters for the ternary blend were determined based on values our group had previously

Table 1 Extrusion parameters

Blends	Zone 1	Zone 2	Zone 3	Zone 4	Zone 5	Zone 6	Cooling method
75 PCL 25 TPU	155	170	170	170	170	170	Water quenched
50 PCL 50 TPU	180	180	180	180	180	180	Air
25 PCL 75 TPU	175	175	175	175	175	175	Air
PLA/PCL/TPU	150	180	180	180	175	175	Air

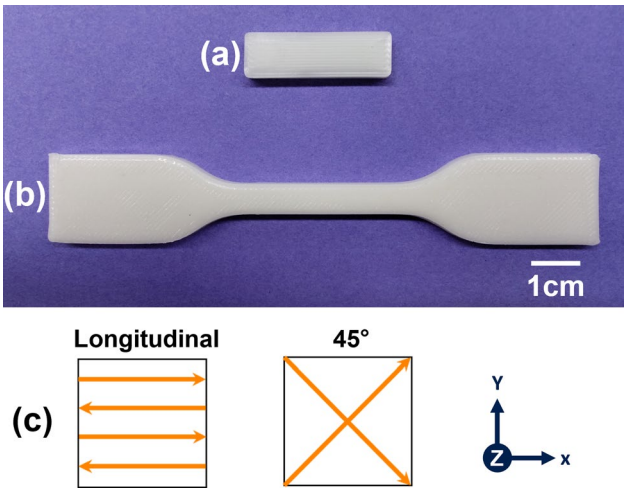

Figure 2 Example of **a** DMA specimen and **b** Type IV tensile specimen fabricated by FFF and **c** depiction of the print raster patterns used in this study.

Table 2 FFF print temperatures

Printer settings	75 PCL 25 TPU (°C)	50 PCL 50 TPU (°C)	25 PCL 75 TPU (°C)	PLA/ PCL/TPU (°C)
Bed temperature	50	50	50	50
Nozzle temperature	210	220	225	210

determined for a blend composed of PLA and TPU and these parameters are documented in literature [6].

Two main types of specimens were used in this study, a tensile test specimen based on the ASTM D638 Type IV geometry [32] and a specimen for dynamic mechanical analysis (DMA). Specimens were fabricated by FFF (Fig. 2) with a Lulzbot Taz 5 (Fargo, North Dakota, USA) with a 0.5 mm diameter nozzle. The FFF parameters were determined based on works performed by our group and others with blends of similar compositions [5, 6, 33] and are listed in Table 2. Two print raster patterns were used, a longitudinal raster pattern where the print rasters were in the direction of the length of the specimen and a crisscross pattern where the print raster direction alternated by 45° for each layer (Fig. 1c). The initial testing of the binary blends only involved the longitudinal raster pattern as previous work has shown this pattern yields optimum results in terms of tensile testing and shape memory performance [2, 5]. As will be seen later, the best-performing binary blend in terms of tensile and shape memory properties was the 50/50 by mass ratio blend of PCL and TPU. Once the decision was made to focus on equal parts by mass ratio blends, the 45° raster pattern was also incorporated into this study to determine the effect of raster pattern on the physical properties. The printed samples were stored in zip bags with desiccant to avoid any hygroscopic damage due to moisture, which can prove to deteriorate mechanical properties of polyester materials [34].

Analysis by DMA was carried out with a PerkinElmer DMA 8000 (PerkinElmer, Waltham, MA, USA). Tensile testing was performed using a MTS Criterion C-44 tensile testing machine equipped with a 10 kN load cell and an Advantage™ Model AHX 800 extensometer (MTS Systems Corporation, Eden Prairie, MN, USA). In general, our procedure for determining the shape memory properties has been to hold specimens at 100% elongation under load for a period of 5 min and then recover the specimens near or at the temperature at which the max tan δ was observed during DMA testing [2, 5]. The sample pool size for the tensile testing of all materials was 5 specimens.

The crystallinity of the material systems was characterized using X-ray diffraction (XRD). The instrument used was a Bruker D8 Discover XRD (Madison, Wisconsin, USA). The X-rays used were Cu Kα (λ = 1.54 Å), and the scan increment was 10° to 40° on the 2θ scale. The emitter side of the instrument was outfitted with a slit 0.2 mm in width, while the detector side had no slit. Scanning electron microscopy (SEM) was used to examine the fracture surfaces of selected mechanical test specimens. The instrument used was a Hitachi SU 3500 SEM (Hitachi High Technologies America, Dallas, TX, USA) equipped with a backscatter electron detector (BSE) as well as an ultra-variable pressure detector (UVD). To mitigate the effects of charging common with non-conductive specimens, the instrument was operated in variable pressure mode at 40 Pa. Additionally, the instrument was operated with an accelerating potential of 10 kV. A Hitachi H-9500 transmission electron microscope (TEM) was used to characterize the mixing of constituents for select blends. The instrument was operated with an accelerating potential of 100 kV. Specimens were fabricated for TEM analysis by way of cryo-ultramicrotomy using an RMC PT-X ultramicrotome (Boeckeler Instruments, Tucson AZ, USA) equipped with a CR-X cryo-sectioning unit. Cutting of the thin sections was achieved using an RMC wet cryo diamond knife with a boat filled with a mixture of 60:40 by volume dimethyl sulfoxide (DMSO)

and ethanol (EtOH). The blade was held at a temperature of − 25 °C, while the specimen was held at a temperature of − 90 °C with the aid of liquid nitrogen.

Shape memory characterization was carried out by considering the as-printed condition as the permanent shape. Specimens were pulled uniaxially to 100% elongation (ε_m) at room temperature in the tensile test machine and held under load for 5 min. Once the specimen was removed, the percent elongation was measured (ε_u). In a previous study involving the characterization of shape memory polymer blends performed by Quiñonez et al. [5] we had demonstrated the use of DMA testing to determine the recovery temperature where the temperature at which max tan δ occurred was used to recover specimens to the original shape after deformation. In the work presented here, the temperature used to recover the specimens was 65 °C, which was near (± 6 °C) the max tan δ temperature for all materials tested. The specimens were subjected to the recovery temperature by placing them in a horizontal air flow oven (Model 3.65, VWR International, Radnor, PA, USA) for 5 min. The elongation of the recovered specimens (ε_p) was measured after removing the specimens from the oven and allowing them to cool to room temperature. The shape memory parameters, namely R_r and R_f, were calculated by inserting the measured values into Eq. (1) and Eq. (2).

Results

DMA testing

As mentioned previously, we have used DMA to determine the temperature at which max tan δ occurs and then use this value as the shape recovery temperature for shape memory testing [2, 5]. We have the same in the work presented here and also made observations pertinent to the testing of AM fabricated specimens as well as observations related to constituent content. In the case of the binary blends composed of TPU and PCL, the DMA graphs (Fig. 3) indicate a difference in dampening characteristics due to a variation in the PCL content. As the PCL concentration was lowered the blend exhibited more energy return, essentially behaving more like a spring, as indicated by a decrease in the max tan δ which, in turn, is driven by a greater loss modulus ($E\varepsilon$) [35, 36]. The temperature

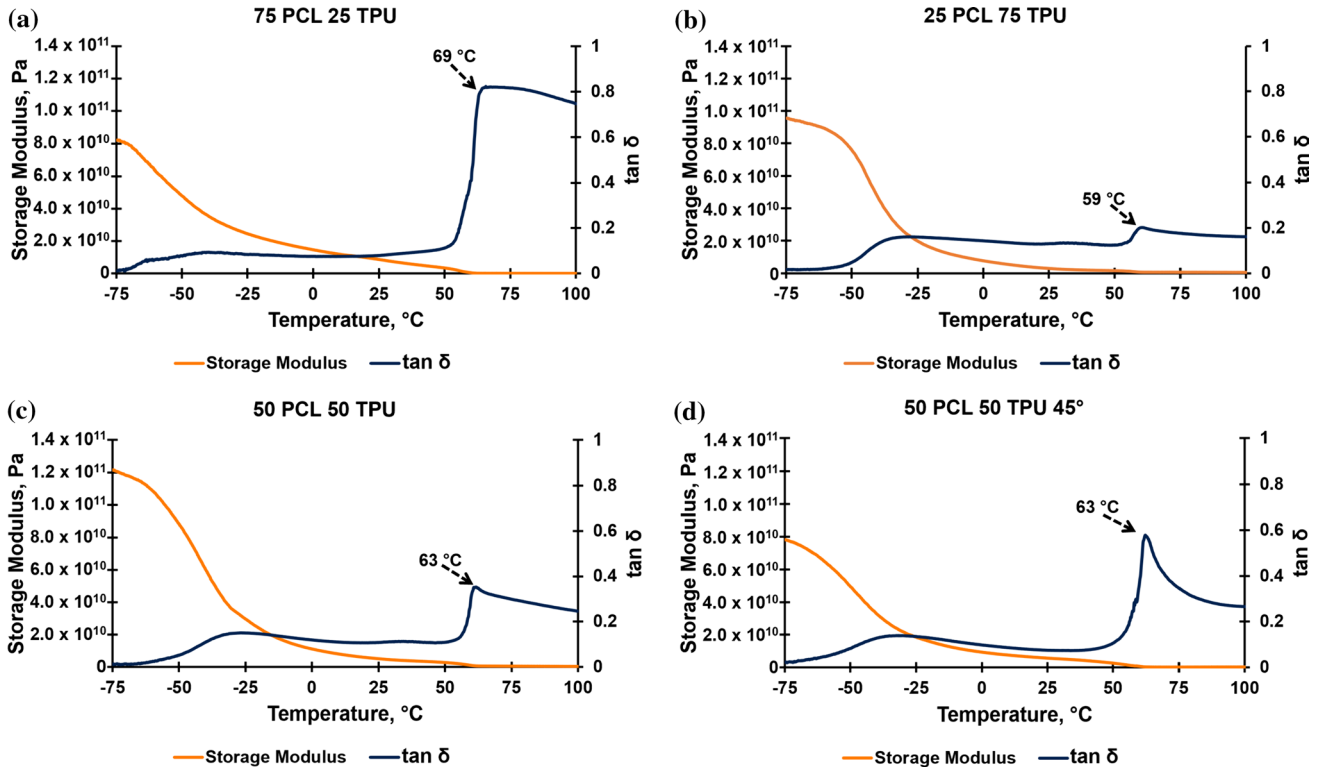

Figure 3 DMA graphs for the PCL/TPU binary blends **a** 75/25 by mass PCL/TPU, **b** 25/75 by weight PCL/TPU, **c** 50/50 by mass PCL/TPU and **d** 50/50 by mass PCL/TPU printed in a 45° raster pattern.

where the max tan δ was observed did not vary linearly with PCL content, but as mentioned before all temperatures were ± 6° of 65°. It should also be noted that the glassy onset temperatures as indicated on the storage modulus curve for the binary blends were well below 0 °C as would be expected as PCL and TPU have T_g values below this temperature with PCL and TPU having T_g values on the order of − 60 and − 23 °C, respectively [37, 38]. The initial specimens for DMA were printed in the longitudinal raster pattern. Once it was decided to pursue the compounding of equal parts by mass blends, the DMA analysis was repeated for the 45° raster pattern, like our strategy for tensile testing. This was done because previous work by our group has shown that raster pattern has an effect on DMA results [5, 39]. Comparing the max tan δ values between the longitudinal and 45° raster patterns showed an increase in the value from 0.35 to 0.57 between the two indicating that raster pattern influences dampening properties. In the case of the ternary PCL/TPU/PLA blend, the effect of the PLA addition is obvious from the DMA graph as the tan δ curve is much more pronounced. Additionally, a secondary glassy onset temperature is observable at 50 °C (Fig. 4); however, this secondary onset is not as obvious for the 45° raster pattern. Comparing the max tan δ between the two raster patterns showed an inverse behavior as compared to the binary blend as the longitudinal raster pattern yielded a max tan δ value of 0.99 while the 45° pattern produced a value of 0.80, again showing that raster pattern influences dampening, but the influence will depend on the material being tested. The results of DMA testing are listed in Table 3.

Tensile testing

Comparing the mechanical testing results between the binary blend concentrations (Fig. 5) reveals that the 50/50 by mass ratio PCL/TPU blend yielded the greatest UTS values (34.4 ± 1.3 MPa). The 50/50 blend also yielded the greatest % elongation values among the binary blends (1972.5 ± 34.9%). Again, the initial comparison was made using a longitudinal raster pattern. Based on the finding that the 50/50 blend yielded the greatest mechanical properties, we then fabricated specimens with a 45° raster pattern. Comparing the

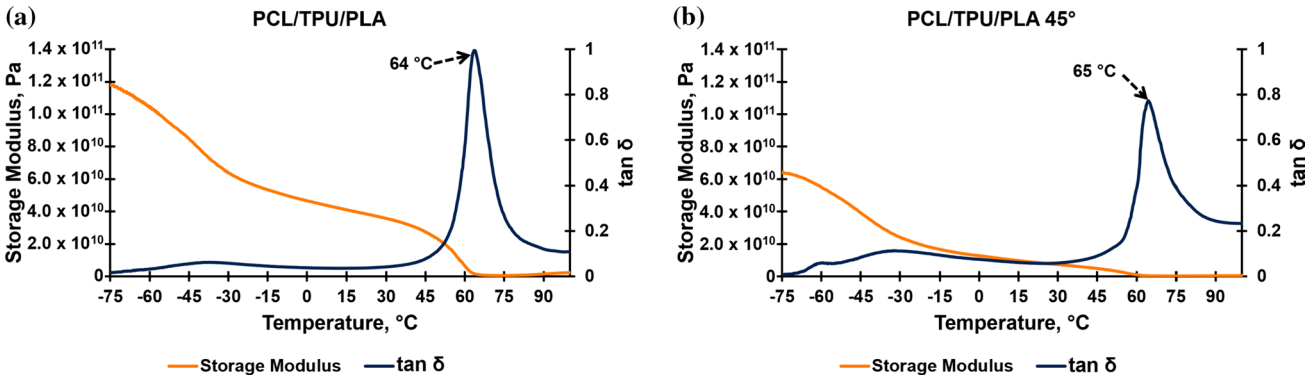

Figure 4 DMA graphs for the ternary blend composed of equal parts by mass PCL, TPU and PLA for **a** specimen printed in the longitudinal raster pattern and **b** specimens printed in the 45° raster pattern.

Table 3 DMA Results

Experimental group	Max tan δ	Max tan δ temp (°C)	Storage modulus at glassy onset	Glassy onset temp (°C)
75 PCL/25 TPU	0.85	69	8.00×10^{10} Pa	− 75
50 PCL/50 TPU Long	0.35	63	1.18×10^{11} Pa	− 70
50 PCL/50 TPU 45°	0.57	63	7.19×10^{10} Pa	− 65
25 PCL/75 TPU	0.20	59	8.30×10^{10} Pa	− 55
PLA/PCL/TPU Long	0.99	64	2.51×10^{10} Pa	49.8
PLA/PCL/TPU 45°	0.80	65	6.00×10^{10} Pa	− 65

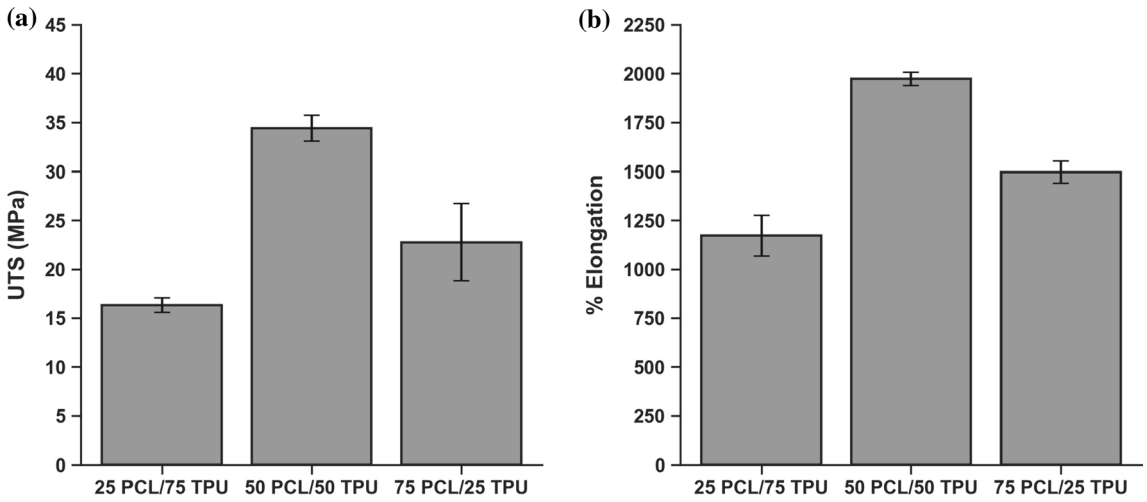

Figure 5 Mechanical testing values for the various iterations of the PCL/TPU blend **a** UTS values and **b** %El values.

tensile test results of the 45° and longitudinal raster pattern showed that the UTS dropped by a statistically significant amount from 34.4 ± 1.3 MPa to a value of 26.5 ± 3.7 MPa, which is greater than the error; however, the %El values were statistically the same at 1961.7 ± 50.6% and 1972.5 ± 34.9% for the 45° and longitudinal raster patterns, respectively (Fig. 6).

As mentioned previously, the finding that the equal parts by mass blend of PCL and TPU yielded the best mechanical property results motivated the development of a ternary blend with equal parts by mass, following a strategy employed in the creation of high entropy material systems. The PCL/TPU/PLA blend was also subjected to tensile testing where two raster patterns were evaluated. When comparing the mechanical properties of this ternary blend (Fig. 7), it was found that the 45° raster pattern yielded greater values in both UTS and %El. In terms of UTS, the 45° raster pattern yielded values of 30.3 ± 0.9 MPa for the longitudinal raster pattern and 35.9 ± 2.0 MPa for the 45° raster pattern. The %El values were also greater for the 45° raster pattern with a value of 857.3 ± 14.7% compared to 626.0 ± 93.9% for the longitudinal raster pattern. This was an unexpected result and could indicate that the ternary blend has a greater propensity to resist shear as the 45° raster pattern effectively puts the

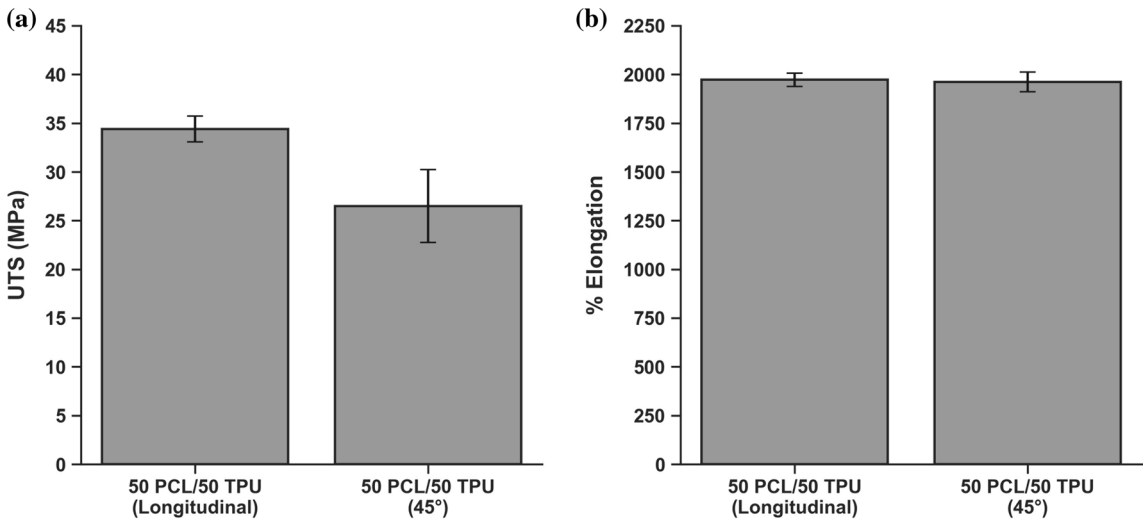

Figure 6 Comparison of the testing values for the 50/50 PCL/TPU blend printed in the longitudinal and 45° raster pattern **a** UTS values and **b** %El values.

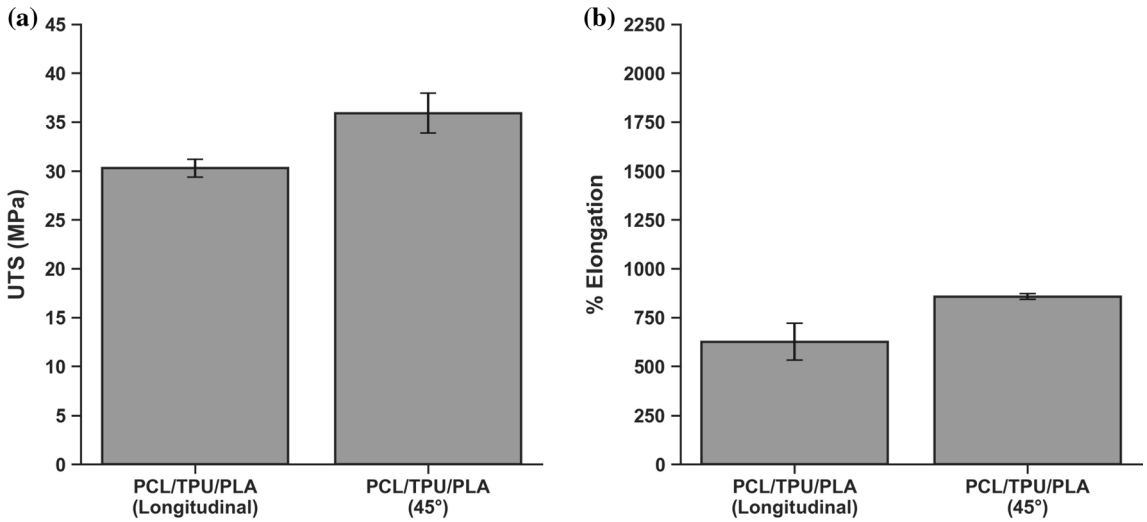

Figure 7 Comparison of the testing values for the ternary PCL/TPU/PLA blend printed in the longitudinal and 45° raster pattern **a** UTS values and **b** %El values.

individual rasters in a state of shear during a tensile test as the individual print rasters are oriented 45° to the direction of applied stress of the tensile test as has been described elsewhere by Dave et al. [40]. Additionally, as we have noted in previous raster pattern studies performed by Lares et al. [39] that the shear caused by the 45° raster pattern coupled with the strain rate of 10^{-2} led to the manifestation of adiabatic shear bands in specimens fabricated from PLA.

SEM microanalysis

Analysis of the fracture surfaces of tensile specimens revealed that the failure mode of both the binary and ternary blend was ductile in nature. Delamination between the print rasters caused by strain the specimen endured during the tensile test [41, 42] was prevalent on all of the tensile specimens. Differences between the 45° and longitudinal raster patterns were not distinguishable, as is normally the case with specimens made by FFF. Fractography of the ends of delaminated clusters (Fig. 8) allowed for the analysis of the fracture surface morphology. In the case of the 50/50 PCL/TPU blend (Fig. 8a) fibrils (highlighted by the dashed arrows) can be seen on the ends of the delaminated raster. The end of the delaminated cluster exhibited a large amount of plastic deformation. The dashed box in Fig. 8a is seen at higher magnification in Fig. 8b where the fracture surface is indicative of opened craze cracks [43–45] and resembles that of a more brittle fracture mode. The reason for the more brittle-like fracture morphology is due to the relatively small cross-sectional area of the delaminated cluster [6, 42]. The fracture surface morphology of the 50/50 PCL/TPU blend printed in a 45° raster pattern was also dominated by delamination. Examination of the ends of the delaminated bundle (Fig. 8c) revealed a large amount of plastic deformation where a smaller delaminated strand is highlighted by the dashed white arrow and a fibril (highlighted by the solid white arrow) was also observed.

Specimens fabricated from the ternary blend of PCL/TPU/PLA also exhibited fracture surface features indicative of ductile failure. A representative specimen printed in the longitudinal print raster pattern exhibited some delamination, but to a qualitatively lesser degree than that observed for the binary blends, however, there was some degree of delamination observed in the center of the representative specimen examined by SEM (Fig. 9a). Fibrils can be observed on the edges of the delaminated strands (highlighted by the dashed white arrows in Fig. 9a and b). The fracture surface of the end of a strand reveals similar brittle-like fracture surface morphology, again due to the localized reduction of cross-sectional area (Fig. 9b). The reason for the higher UTS values exhibited by the 45° raster pattern sample pool is obvious from the fracture surface (Fig. 9c)

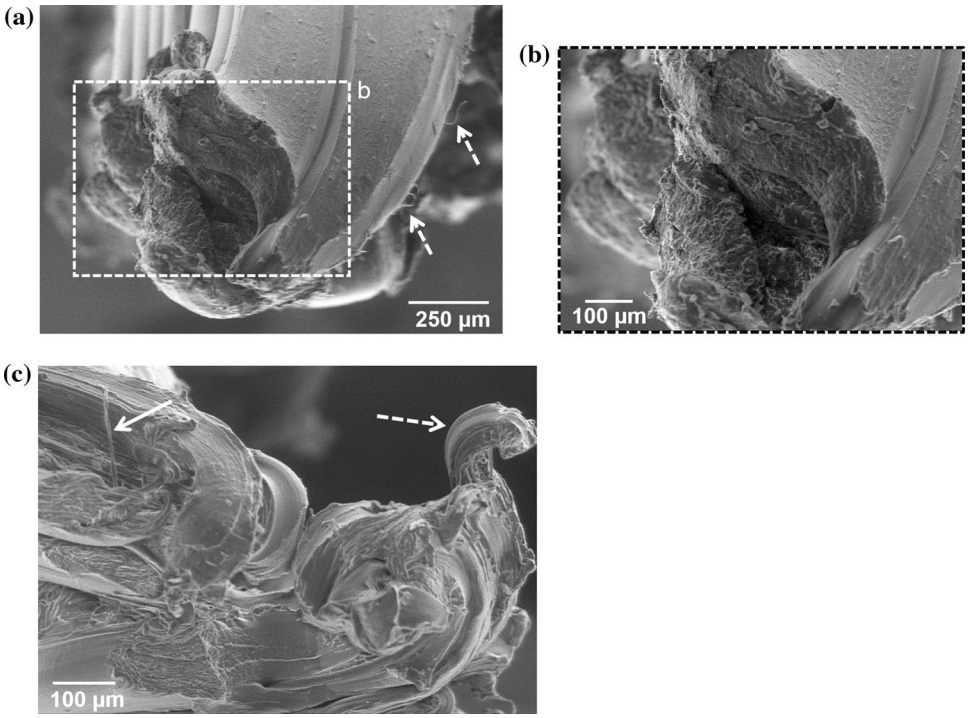

Figure 8 SEM micrographs of **a** and **b** the binary blend of 50/50 PCL/TPU printed in a longitudinal raster pattern and **c** the same blend printed in a 45° raster pattern.

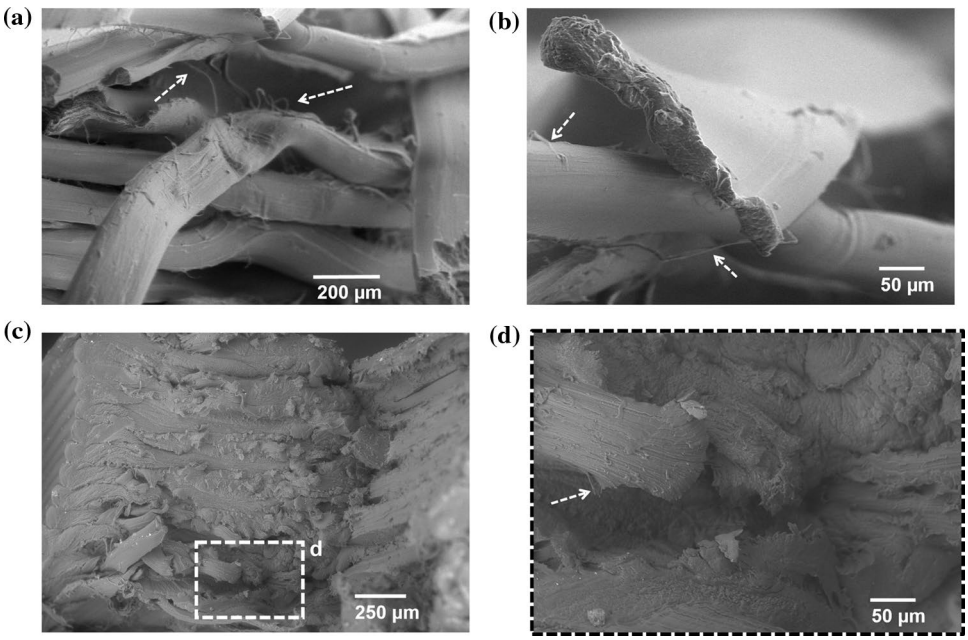

Figure 9 SEM micrographs of **a** and **b** the ternary blend of equal parts by mass PCL, TPU, and PLA printed in a longitudinal raster pattern and **c** and **d** the same blend printed in a 45° raster pattern.

which revealed that the specimen held together during the tensile test. The fracture surface morphology is still ductile in nature, and this is more obvious in the higher magnification image (Fig. 9d) which exhibits a large amount of plastic deformation and a fibril (indicated by the dashed white arrow).

TEM analysis

Transmission electron micrographs of the 50/50 PCL/TPU blend and the ternary PCL/TPU/PLA blend are shown in Fig. 10. The microstructure of the binary blend (Fig. 10a) is indicative of an immiscible blend where two phases are clearly discernable. In the

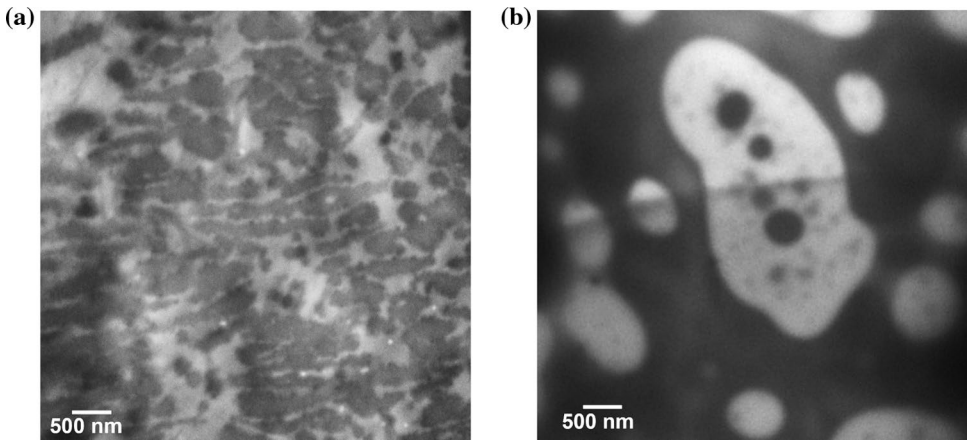

Figure 10 Transmission electron micrographs of **a** the 50/50 by mass binary blend of PCL and TPU and **b** the ternary, equal parts by mass PCL/TPU/PLA blend.

case of the ternary blend (Fig. 10b) three phases are observed also indicating an immiscible blend. Considering that both images are the same magnification, the relative size of the phase domains differs between the binary and ternary blend as the ternary blend formed phase domains of a greater size. The manifestation of an immiscible blend though the δ values of the individual blend constituents are close to one another is consistent with the microstructure observed when blending PLA and TPU seen in previous work by Quiñonez et al. [5].

Shape memory characterization

Specimens were subjected to a shape memory cycle as illustrated by the examples shown in Fig. 10, allowing for calculation of the critical parameters (R_r and R_f). The specimens in Fig. 10 are of different iterations of the PCL/TPU binary blends. Comparing the measurements of the binary blends, (Fig. 11) the 50/50 by mass ratio exhibited the greatest R_r values (99.9 ± 0.4%). We do acknowledge that the error technically indicates sample shrinkage, but we attribute this to potential error in the manual measurement caused by distortion of the specimens during the SMP cycle. We also note that the 75/25 blend of PCL and TPU exhibited the greatest overall shape memory parameters as determined by comparison of the SMI values, however, the relatively low values observed during the mechanical testing results as well as the difficulty in printing the material due to the stickiness led us to discount this blend iteration and focus on the equal part by mass blend of 50/50 PCL and TPU. Additionally, the 75/25 blend specimens did not fully recover from necking

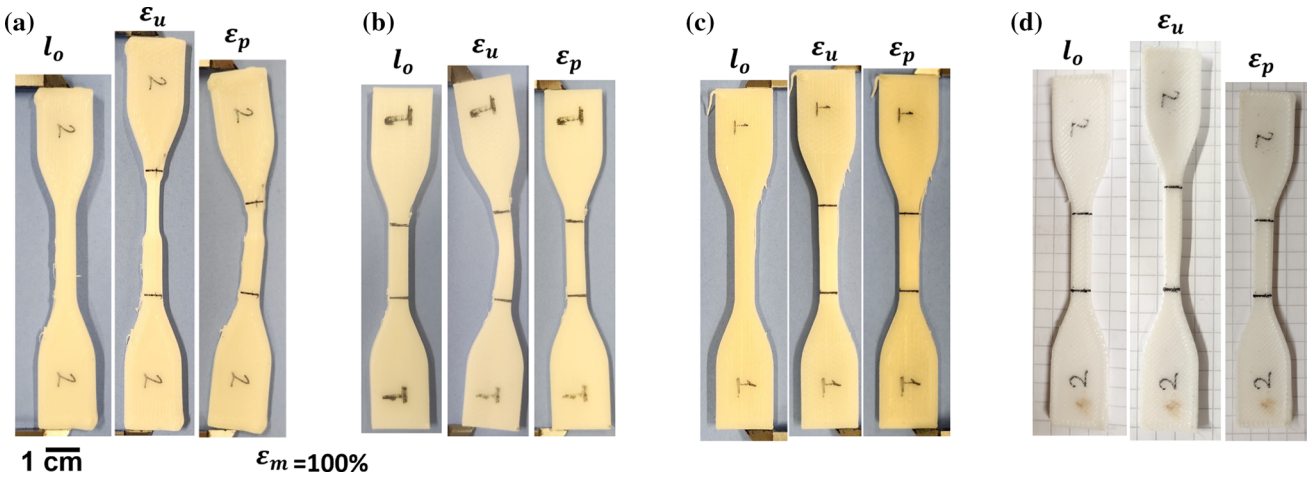

Figure 11 Representation of the calculation of the shape memory parameters for binary blends of PCL/TPU for the **a** 75/25, **b** 50/50, **c** 25/75 blend ratios printed in a longitudinal raster pattern and **d** the 50/50 blend printed in a 45° raster pattern.

that occurred during the tensile test (Fig. 11a). Though the 50/50 blend specimens exhibited bowing upon unloading, the deformation disappeared after thermal recovery (Fig. 11b). The 25/75 by mass ratio blend of PCL and TPU did not exhibit distortion; however, this iteration of the binary blend did not exhibit good shape fixation or shape recovery properties (Figs. 11c and 12). A shape memory test was also performed on 50/50 PCL/TPU specimens fabricated in the 45° raster pattern, and no distortion of the specimens was observed after removal from the tensile test machine (Fig. 11d). Also, both the R_r and R_f parameters and consequently, the SMI were statistically equal to the longitudinal raster pattern as is seen in the graphical representation of the shape memory values in Fig. 12. The values for shape fixation and shape recovery for the binary blend systems are listed in Table 4 and agree with values presented by Pinto, et al. [21] who also investigated the shape memory properties of PCL/TPU blends.

Shape memory testing was also carried out for the ternary blend composed of PCL, TPU, and PLA. For samples printed in the longitudinal raster pattern, the SMI was a higher value than any of the binary blends (98.8 ± 0.6%); however, considering that R_r values were 100.7 ± 0.07%, some shrinkage of the specimens occurred during the recovery process. In the case of the specimens printed in the 45° raster pattern, the SMI was slightly greater 99.4 ± 0.6% with a recovery ratio of 99.4 ± 0.05% indicating that the raster pattern influences the propensity of specimens to shrink. We believe that the shrinkage, albeit a negligible amount, is due to the polymer chains aligning in the direction of applied strain during the tensile test and then kinking as crystallization occurs during the recovery process. Additionally, we have noted shrinkage of specimens in other PLA-containing shape memory polymeric systems [6]. The high SMI values were also indicative of the ability of the ternary blend to hold a temporary shape as was also directly measured by

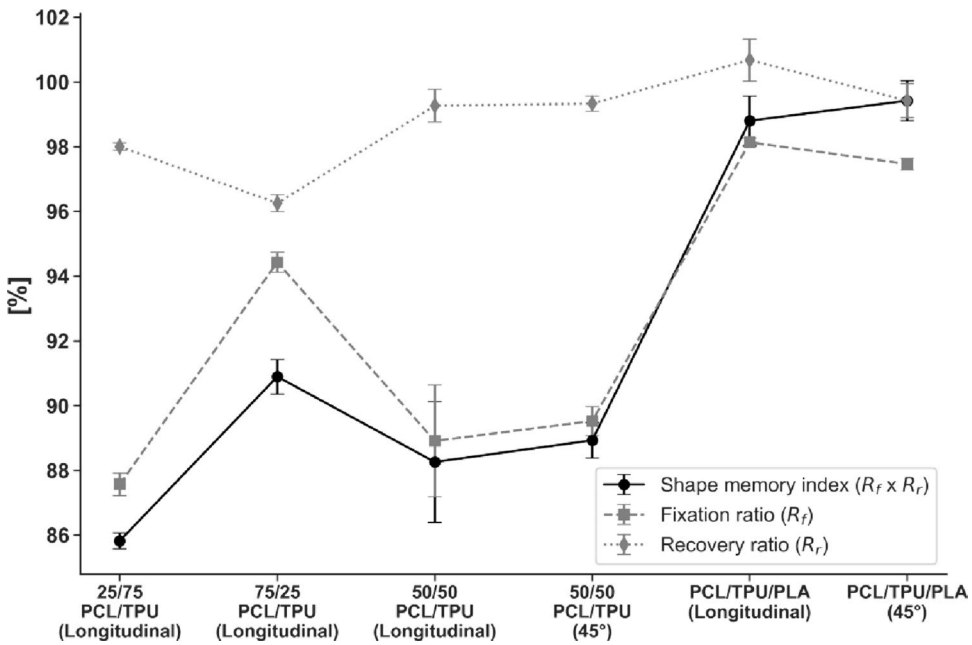

Figure 12 Graphical representation of the critical shape memory values for all blends evaluated in this study.

Table 4 Shape memory testing results

Blend	R_f (%)	σ	R_r (%)	σ	SMI (%)	σ
25/75 PCL/TPU (Longitudinal)	87.57	0.35	98.01	0.11	85.83	0.25
75/25 PCL/TPU (Longitudinal)	94.43	0.31	96.25	0.26	90.90	0.54
50/50 PCL/TPU (Longitudinal)	88.91	1.73	99.27	0.50	88.26	1.87
50/50 PCL/TPU (45°)	89.53	0.45	99.33	0.24	88.93	0.55
PCL/TPU/PLA (Longitudinal)	98.14	0.14	100.68	0.65	98.81	0.77
PCL/TPU/PLA (45°)	97.47	0.18	99.42	0.52	99.42	0.62

the R_f values of 98.1 ± 0.1% for the specimens printed in the longitudinal direction and 97.5 ± 0.2% for the specimens printed in the 45° raster pattern. Examples of the shape memory testing for the ternary blend of PCL/TPU/PLA blend are shown in Fig. 13.

In general, two mechanisms can be used to define the shape memory properties in a polymer blend: (1) dual state, where the temporary shape is maintained by weak crosslinks and the permanent shape is held by covalent bonds; and (2) dual component where hard and soft components are responsible returning to the permanent shape and holding a temporary shape, respectively [5, 46]. We describe the mechanisms for the shape memory polymer blends studied here based on the combination of the two mechanisms. Within a macromolecule of TPU, there are hard and soft segments [21, 47], making this a dual component SMP, whereas PCL and PLA are driven by the dual state mechanism. For blends with a higher amount of dual state mechanism-driven material (% by mass PCL in the ternary blend and the ternary blend essentially being 66% by mass dual state shape memory polymer), the SMI is the greatest meaning that the dual state is a more efficient shape memory mechanism than dual component. Additionally, as mentioned before, PLA is a robust shape memory polymer, and the results of the shape memory performance of the ternary PCL/TPU/PLA blend are similar to values documented by Quiñonez et al. [5] for shape memory blends composed of PLA and TPU.

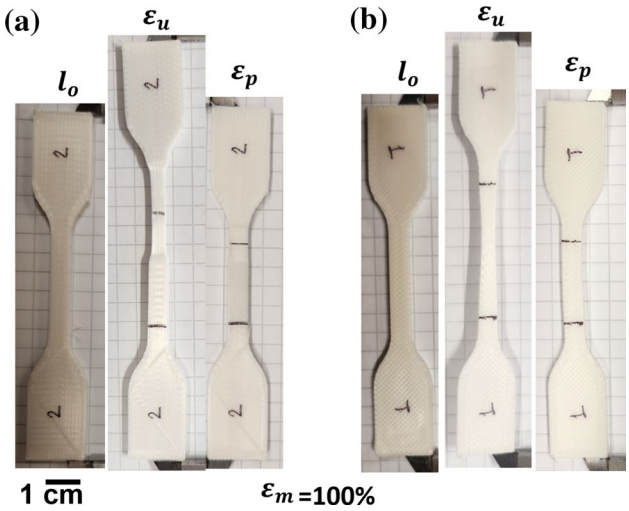

Figure 13 Representation of the calculation of the shape memory parameters for ternary blends of PCL/TPU/PLA for the **a** specimens printed in the longitudinal raster pattern and **b** specimens printed in the 45° raster pattern.

To determine the effect of recovering from plastic deformation on the strength of our materials, the specimens for the 50/50 PCL/TPU and PCL/TPU/PLA blends were again subjected to a tensile test and pulled to failure after thermal recovery. Compared to the baseline UTS data, the PCL/TPU blend exhibited UTS values that were greater than the error as compared to baseline specimens for both the longitudinal and 45° raster patterns (Fig. 14). Applying a Tukey–Kramer honest significant difference (HSD) test revealed the difference in strength to be statistically significant (Fig. 15). The ternary blend specimens pulled to failure after the SMT exhibited a decrease in strength, but the difference was within the standard deviation.

We believed that the increase in strength for the binary blend was due to the manifestation of crystalline domains within the material during the shape memory cycle. Both PCL and PLA are semicrystalline polymers [17, 48] so some level of crystallinity would be expected in the binary and ternary blends.

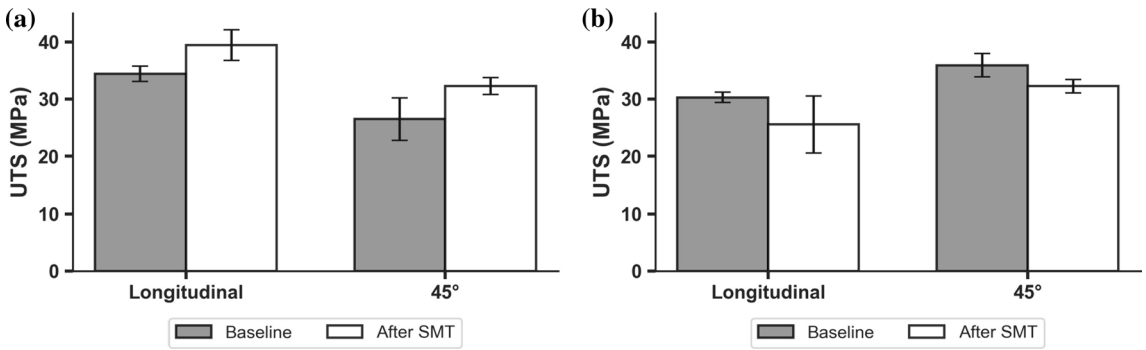

Figure 14 Comparison of the UTS values for **a** the 50/50 PCL/TPU blend and **b** the ternary PCL/TPU/PLA blend for baseline specimens and tensile specimens that were pulled to failure after being subjected to a shape memory test cycle.

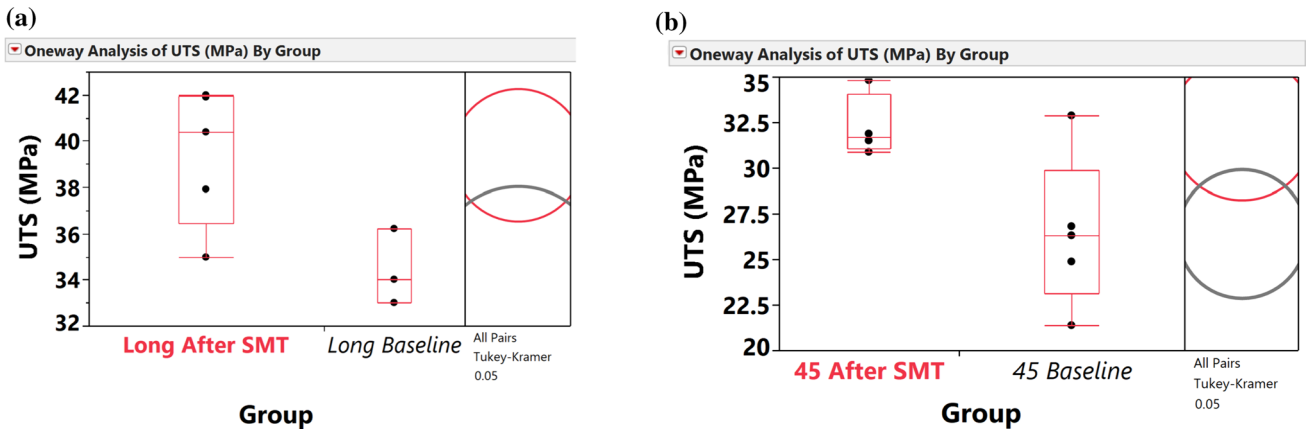

Figure 15 Tukey–Kramer HSD test showing that the increase in strength for 50/50 PCL/TPU specimens pulled to failure after shape memory testing was statistically significantly greater than the UTS values for baseline specimens where the raster pattern was **a** longitudinal and **b** 45°.

To further elucidate the mechanism of strengthening, specimens in the as-printed (control), stretched, and recovered state were subjected to analysis via XRD. A fourth specimen was included that was an as-printed specimen which was annealed at the same time and temperature conditions as the recovery process. This was done to separate thermally induced crystallinity from strain-induced crystallinity. In this experiment, we used smaller ASTM D638 Type V tensile specimens printed in the longitudinal raster pattern. The XRD spectra are shown in Fig. 16. In the case of the binary blend, both the as-printed and the stretched specimen exhibited little to no crystallinity. Annealing produced two prominent peaks near the known locations for the (110) and (200) peaks for PCL (~ 21.2 and 23.4°, respectively) [49]. The slight shift of the peaks to the left (smaller angles) for the annealed and as-printed spectra is indicative of less structural order, meaning that the full cycle increased the order of crystallinity. The specimen subjected to the total shape memory test (deformation followed by thermal recovery) exhibited peaks at roughly 21.3°, 21.9°, and 23.6°, which are the known peaks for (110), (111), and (200) reflections for PCL crystallized in the orthorhombic structure [50, 51]. We emphasize here that the total shape memory cycle led to the manifestation of crystalline domains in a greater amount as compared to specimens in the as-printed and annealed states and we attribute this larger amount of crystallized domains to the increase in strength observed when pulling cycled specimens to failure as compared to the baseline specimens. The increase in crystallinity is evident by the increase in the relative intensity of the peaks and the appearance of the (111) reflection for the recovered specimen.

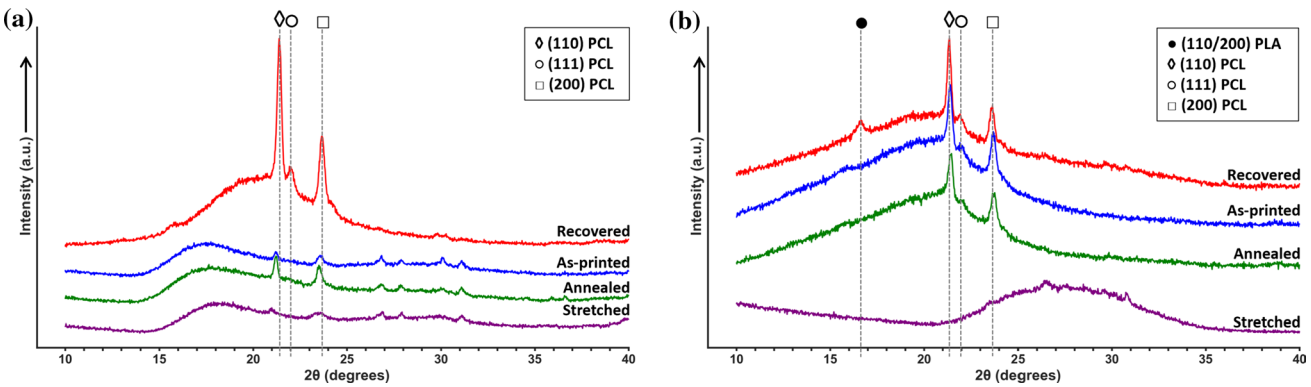

Figure 16 XRD spectra for **a** the binary PCL/TPU blend at a 50/50 by mass ratio and **b** the PCL/TPU/PLA ternary blend. The states at which the scans were made are indicated on the individual spectra and the distinct peaks are indicated by unique symbols.

We can infer from these data that the PCL constituent or rather an increase of the number of crystallized domains within this constituent is the mechanism of strengthening.

The influence of PCL content was also notable when comparing the spectra for the ternary PCL/TPU/PLA blend (Fig. 16b) in the as-printed, stretched, annealed, and recovered states. The (110), (111), and (200) reflections of PCL are visible in the spectra for the as-printed control, annealed and recovered specimens. Stretching the material effectively de-crystalized the material and a large amorphous halo manifested between ~ 21.2° and 34.5°. The full recovery cycle also led to the manifestation of crystalline domains in the PLA phase as the known location for the (110/200) peak is visible at 16.6° [17, 52, 53]. The location of the (110/200) peak of PLA indicates that the domains also crystallized in the orthorhombic crystal structure [54]. Though PCL also crystallizes in the orthorhombic structure the smaller angle for both the (110) and (200) reflections indicates the *d*-spacing of PLA to be larger. This means that the shape memory cycle renders the ternary blend a semi-polycrystalline material where the different size crystalline domains will deform at different rates. We believe that this is the reason that no strengthening is realized after the shape memory cycle as was the case with the binary blend. Our observations and deductions are consistent with published values for the lattice parameters of PCL ($a = 7.48$ Å, $b = 4.98$ Å, and $c = 17.26$ Å) [51] and PLA ($a = 10.08$ Å, $b = 5.90$ Å, and $c = 28.70$ Å) [54]. Considering that the equation used to calculate the *d*-spacing for an orthorhombic crystal can be expressed as:

$$\frac{1}{d_{hkl}} = \frac{h^2}{a^2} + \frac{k^2}{b^2} + \frac{l^2}{c^2} \tag{4}$$

the *d*-spacing for the (200) plane would be 3.74 Å and 5.04 Å for PCL and PLA, respectively. Based on the same parameters, the *d*-spacing for the (110) plane would be 4.14 Å and 5.09 Å for PCL and PLA, respectively. We note there that due to the lattice parameters of PLA, the *d*-spacing for (110) and (200) is extremely hard to distinguish, which is why the peak at 16.6° on the 2θ scale is indexed as (110/200). We also note, that if one were to solve for the Bragg angle (θ) using Bragg's law:

$$\lambda = 2d \sin\theta \tag{5}$$

where λ is the wavelength of the X-rays in the instrument, that the 2θ value is greater for PLA than those seen on our spectra and those published elsewhere [17, 52, 54]. Again, we attribute the shift of reflections to smaller angles to a lower order of crystallinity than that of a material with a larger amount of crystalline domains. In contrast, the PCL exhibited a higher order of crystallinity than the PLA in the case of the recovered specimens as indicated by both the higher relative intensity of the peaks as well as the values for solved Bragg angles more closely matching those observed on the spectra. A potential reason for the full deformation and recovery cycle leading to the manifestation of a greater amount of crystalline domains is that when the specimen is stretched during the tensile test, the polymer chains within the specimen become elongated and oriented in the same direction [55]. The elongated state then makes it easier for the polymer chains to fold into crystalline domains during the recovery process [56]. Considering the shape memory test as a thermomechanical cycle, the increase in crystallinity as indicated by XRD spectra is consistent with work performed by Quiñonez et al. [5] who observed crystalline peaks on FFF made PLA/TPU blend specimens that were subjected to DMA testing.

Conclusions

In the work presented here, we developed binary and ternary shape memory polymer blends for the FFF additive manufacturing method. The blend constituents were chosen because they were all from the same polymer family (all are polyesters), had similar Hildebrand solubility parameters and all had inherent shape memory properties. Though the constituents of the blends studied here were similar, microanalysis via TEM showed the resulting mixtures to be immiscible as indicated by the observation of two distinct phases in the case of the binary blend and three distinct phases in the case of the ternary blend. Comparing the phase morphology of the 50/50 PCL/TPU blend with the PCL/TPU/PLA blend revealed the latter to produce phases with larger domain sizes.

A key finding of this work was that the 50/50 PCL/TPU blend exhibited self-strengthening capabilities. Further experiments involving XRD revealed the strengthening mechanism to be the formation of crystalline domains caused by the thermomechanical shape memory test cycle which led to the

manifestation of a greater number of crystalline domains than annealing the specimens alone. A key result was also observed for the ternary PCL/TPU/PLA blend where the 45° raster pattern exhibited higher UTS values as compared to the longitudinal raster pattern. This may indicate that the ternary blend is more resistant to shear as compared to the binary blend as others have noted that the 45° raster pattern subjects the individual print rasters in a greater state of shear as compared to the longitudinal raster pattern.

In terms of shape memory performance, in the case of the three binary blends evaluated here, the blend with the highest PCL content (75% by mass) exhibited the best shape memory performance. However, the ternary blend exhibited more optimal shape memory characteristics than any of the binary PCL/TPU iterations. The better shape memory performance of the ternary blend is most likely driven by the PLA content. Also, considering that the shape memory property of TPU is driven by the dual component shape memory mechanism and that both PCL and PLA are driven by the dual state shape memory mechanism, the results here indicate that the dual component mechanism to be the more robust of the two.

The development of shape memory polymer blends based on the materials selection criteria of solubility parameter, polymer structure, and polymer family (polyester, polyolefin, etc.) allows for the creation of multi-constituent blends without the need for compatibilizers. In this work, we presented the successful combination of three different polyesters, PCL, TPU, and PLA, but we believe this strategy could also be used to create high entropy polymer blends where the constituent amount would be five. The materials design approach presented here could be beneficial to additive manufacturing and the multitude of fields that utilize this fabrication technique.

Acknowledgements

The work presented here was performed in the Polymer Extrusion Lab in the Department of Metallurgical, Materials and Biomedical Engineering (MMBME) at The University of Texas at El Paso (UTEP). The authors are thankful for the use of the XRD, TEM, and tensile tester available in the MMBME department. Funding was provided by the National Science Foundation (NSF) under grant number CMMI 2227573.

Author contributions

Luis E. Lares Carillo fabricated specimens, performed experiments, compiled data, and wrote original manuscript. Yareli O. Gonzalez performed experiments, plotted data, and created figures. Marilyn Parga performed experiments and created figures. Katia Lizbeth Delgado Ramos performed experiments and compiled data. Nadya Neparko fabricated specimens and performed experiments. David A. Roberson conceptualized experiments, performed cryo-ultramicrotomy and TEM analysis, and compiled final manuscript.

Data availability

Not applicable.

Declarations

Conflicts of interest The authors declare no conflicts of interest.

Ethical approval Not applicable.

References

[1] Avila JM, Cavender-Word TJ, Roberson DA (2023) Exploring the effect of moisture exposure on shape memory polymer performance. J Polym Environ. https://doi.org/10.1007/s10924-023-02818-w

[2] Andrade Chávez F, Siqueiros JG, Carrete IA et al (2019) Characterisation of phases and deformation temperature for additively manufactured shape memory polymer components fabricated from rubberised acrylonitrile butadiene styrene. Virtual Phys Prototyp 14:188–202. https://doi.org/10.1080/17452759.2018.1550694

[3] Delaey J, Dubruel P, Van Vlierberghe S (2020) Shape-memory polymers for biomedical applications. Adv Funct Mater 30:1909047. https://doi.org/10.1002/adfm.201909047

[4] Sabahi N, Chen W, Wang C-H et al (2020) A review on additive manufacturing of shape-memory materials for biomedical applications. JOM 72:1229–1253. https://doi.org/10.1007/s11837-020-04013-x

[5] Quiñonez PA, Ugarte-Sanchez L, Bermudez D et al (2021) Design of shape memory thermoplastic material systems

for FDM-type additive manufacturing. Materials 14:4254. https://doi.org/10.3390/ma14154254

[6] Cavender-Word TJ, Roberson DA (2023) Development of a resilience parameter for 3D-printable shape memory polymer blends. Materials 16:5906. https://doi.org/10.3390/ma16175906

[7] Word TJ, Guerrero A, Roberson DA (2021) Novel polymer materials systems to expand the capabilities of FDM™-type additive manufacturing. MRS Commun 11:129–145. https://doi.org/10.1557/s43579-021-00011-5

[8] Lendlein A, Langer R (2002) Biodegradable, elastic shape-memory polymers for potential biomedical applications. Science 296:1673–1676. https://doi.org/10.1126/science.1066102

[9] Lai S-M, Lan Y-C (2013) Shape memory properties of melt-blended polylactic acid (PLA)/thermoplastic polyurethane (TPU) bio-based blends. J Polym Res 20:140. https://doi.org/10.1007/s10965-013-0140-6

[10] Zhang H, Wang H, Zhong W, Du Q (2009) A novel type of shape memory polymer blend and the shape memory mechanism. Polymer 50:1596–1601. https://doi.org/10.1016/j.polymer.2009.01.011

[11] Wang Y, Zhang J, Li M et al (2022) 3D printing thermo-responsive shape memory polymer composite based on PCL/TPU blends. J Polym Res 29:243. https://doi.org/10.1007/s10965-022-03095-2

[12] Jing X, Mi H-Y, Huang H-X, Turng L-S (2016) Shape memory thermoplastic polyurethane (TPU)/poly(ε-caprolactone) (PCL) blends as self-knotting sutures. J Mech Behav Biomed Mater 64:94–103. https://doi.org/10.1016/j.jmbbm.2016.07.023

[13] Xu X, Fan P, Ren J et al (2018) Self-healing thermoplastic polyurethane (TPU)/polycaprolactone (PCL) /multi-wall carbon nanotubes (MWCNTs) blend as shape-memory composites. Compos Sci Technol 168:255–262. https://doi.org/10.1016/j.compscitech.2018.10.003

[14] Ho KG, Pometto AL, Gadea-rivas A et al (1999) Degradation of polylactic acid (PLA) plastic in costa rican soil and Iowa State University compost rows. J Environ Polym Degrad 7:173–177. https://doi.org/10.1023/A:1022874530586

[15] Roberson DA, Rocha CR, Piñon M (2015) Evaluation of 3D printable sustainable composites. University of Texas at Austin

[16] Myers D, Abdel-Wahab A, Hafeez F et al (2022) Optimisation of the additive manufacturing parameters of polylactic acid (PLA) cellular structures for biomedical applications. J Mech Behav Biomed Mater 136:105447. https://doi.org/10.1016/j.jmbbm.2022.105447

[17] Bermudez D, Quiñonez PA, Vasquez EJ et al (2021) A comparison of the physical properties of two commercial 3D printing PLA grades. Virtual Phys Prototyp 16:178–195. https://doi.org/10.1080/17452759.2021.1910047

[18] Carrete IA, Bermudez D, Aguirre C et al (2019) Failure analysis of additively manufactured polyester test specimens exposed to various liquid media. J Fail Anal Prev 19:418–430. https://doi.org/10.1007/s11668-019-00614-0

[19] Aimar A, Palermo A, Innocenti B (2019) The role of 3D printing in medical applications: a state of the art. J Healthc Eng 2019:e5340616. https://doi.org/10.1155/2019/5340616

[20] Ebrahimi F, Ramezani Dana H (2022) Poly lactic acid (PLA) polymers: from properties to biomedical applications. Int J Polym Mater Polym Biomater 71:1117–1130. https://doi.org/10.1080/00914037.2021.1944140

[21] Pinto LA, Backes EH, Harb SV et al (2024) Shape memory thermoplastic polyurethane/polycaprolactone blend and composite with hydroxyapatite for biomedical application. J Mater Res 39:90–106. https://doi.org/10.1557/s43578-023-01172-w

[22] Shin EJ, Jung YS, Park CH, Lee S (2023) Eco-friendly TPU/PLA blends for application as shape-memory 3D printing filaments. J Polym Environ 31:3182–3196. https://doi.org/10.1007/s10924-023-02799-w

[23] Bhattacharya S, Hailstone R, Lewis CL (2020) thermoplastic blend exhibiting shape memory-assisted self-healing functionality. ACS Appl Mater Interfaces 12:46733–46742. https://doi.org/10.1021/acsami.0c13645

[24] Rocha CR, Perez ART, Roberson DA et al (2014) Novel ABS-based binary and ternary polymer blends for material extrusion 3D printing. J Mater Res 29:1859–1866. https://doi.org/10.1557/jmr.2014.158

[25] Quiñonez PA, Bermudez D, Ugarte-Sanchez L, Roberson DA (2019) Tailoring physical properties of shape memory polymers for FDM-type additive manufacturing. In: Solid freeform fabrication 2019: proceedings of the 30th annual inernational solid freeform fabrication symposium. TMS, Austin, TX USA, pp 843–855

[26] Su S, Duhme M, Kopitzky R (2020) Uncompatibilized PBAT/PLA blends: manufacturability, miscibility and properties. Materials 13:4897. https://doi.org/10.3390/ma13214897

[27] Adamska K, Voelkel A, Berlińska A (2016) The solubility parameter for biomedical polymers—application of inverse gas chromatography. J Pharm Biomed Anal 127:202–206. https://doi.org/10.1016/j.jpba.2016.04.014

[28] Gallu R, Méchin F, Dalmas F et al (2020) On the use of solubility parameters to investigate phase separation-morphology-mechanical behavior relationships of TPU.

Polymer 207:122882. https://doi.org/10.1016/j.polymer.2020.122882

[29] Lares Carrillo L (2023) Additive manufacturing of binary and ternary shape memory polyester blends as a pathway towards high entropy polymer systems. Open Access Theses Diss

[30] Zhou Y, Luo L, Liu W et al (2015) Preparation and characteristic of PC/PLA/TPU blends by reactive extrusion. Adv Mater Sci Eng 2015:1–9. https://doi.org/10.1155/2015/393582

[31] Liu F, Vyas C, Poologasundarampillai G et al (2018) Structural evolution of PCL during melt extrusion 3D printing. Macromol Mater Eng 303:1700494. https://doi.org/10.1002/mame.201700494

[32] ASTM (2014) ASTM D638-14: standard test method for tensile properties of plastics. ASTM

[33] AMFG (2018) TPU 3D printing: A guide to 3D printing flexible parts. In: AMFG. https://amfg.ai/2018/07/23/tpu-3d-printing-guide/. Accessed 19 Mar 2023

[34] Siqueiros JG, Roberson DA (2017) In situ wire drawing of phosphate glass in polymer matrices for material extrusion 3D printing. Int J Polym Sci 2017:e1954903. https://doi.org/10.1155/2017/1954903

[35] Keusch S, Haessler R (1999) Influence of surface treatment of glass fibres on the dynamic mechanical properties of epoxy resin composites. Compos Part Appl Sci Manuf 30:997–1002. https://doi.org/10.1016/S1359-835X(99)00007-X

[36] Shin BY, Han DH (2017) Viscoelastic properties of PLA/PCL blends compatibilized with different methods. Korea-Aust Rheol J 29:295–302. https://doi.org/10.1007/s13367-017-0029-8

[37] Ahmed MF, Li Y, Yao Z et al (2019) TPU/PLA blend foams: enhanced foamability, structural stability, and implications for shape memory foams. J Appl Polym Sci 136:47416. https://doi.org/10.1002/app.47416

[38] Han D, Chen G, Xiao M et al (2018) Biodegradable and toughened composite of poly(propylene carbonate)/thermoplastic polyurethane (PPC/TPU): effect of hydrogen bonding. Int J Mol Sci 19:2032. https://doi.org/10.3390/ijms19072032

[39] Lares Carrillo LE, Salazar JF, Hitter MM et al (2023) The effect of raster pattern and acetic acid exposure on the mechanical and failure properties of additively manufactured PLA and PLA-wood composite specimens. J Fail Anal Prev 23:1298–1312. https://doi.org/10.1007/s11668-023-01681-0

[40] Dave HK, Prajapati AR, Rajpurohit SR et al (2022) Investigation on tensile strength and failure modes of FDM printed part using in-house fabricated PLA filament. Adv Mater Process Technol 8:576–597. https://doi.org/10.1080/2374068X.2020.1829951

[41] Roberson DA, Siqueiros JG (2016) Novel polycarbonate/SEBS-g-MA blend for FDM-type 3D printing. In: Annual technical conference-ANTEC. pp 10–14

[42] Siqueiros JG, Schnittker K, Roberson DA (2016) ABS-maleated SEBS blend as a 3D printable material. Virtual Phys Prototyp 11:123–131. https://doi.org/10.1080/17452759.2016.1175045

[43] Torrado AR, Roberson DA (2016) Failure analysis and anisotropy evaluation of 3D-printed tensile test specimens of different geometries and print raster patterns. J Fail Anal Prev 16:154–164. https://doi.org/10.1007/s11668-016-0067-4

[44] Torrado AR, Shemelya CM, English JD et al (2015) Characterizing the effect of additives to ABS on the mechanical property anisotropy of specimens fabricated by material extrusion 3D printing. Addit Manuf 6:16–29. https://doi.org/10.1016/j.addma.2015.02.001

[45] Perez ART, Roberson DA, Wicker RB (2014) Fracture surface analysis of 3D-printed tensile specimens of novel ABS-based materials. J Fail Anal Prev 14:343–353. https://doi.org/10.1007/s11668-014-9803-9

[46] Yang WG, Lu H, Huang WM et al (2014) Advanced shape memory technology to reshape product design, manufacturing and recycling. Polymers 6:2287–2308. https://doi.org/10.3390/polym6082287

[47] Li H, Gao Y, Zhao S et al (2022) Dual and triple shape memory properties of poly(ε-caprolactone)-based cross-linked polymer elastomers. Polym Test 115:107738. https://doi.org/10.1016/j.polymertesting.2022.107738

[48] Tekay E, Şen S, Korkmaz MA, Nugay N (2023) Preparation and characterization of thermo-responsive shape memory ester-based polymer blends. J Mater Sci 58:8241–8260. https://doi.org/10.1007/s10853-023-08549-6

[49] Borjigin M, Eskridge C, Niamat R et al (2013) Electrospun fiber membranes enable proliferation of genetically modified cells. Int J Nanomed 8:855–864. https://doi.org/10.2147/IJN.S40117

[50] Biscaia SI, Viana TF, Almeida HA, Bártolo PJ (2015) Production and characterisation of PCL/ES scaffolds for bone tissue engineering. Mater Today Proc 2:208–216. https://doi.org/10.1016/j.matpr.2015.04.024

[51] Hu H, Dorset DL (1990) Crystal structure of poly(iε-caprolactone). Macromolecules 23:4604–4607. https://doi.org/10.1021/ma00223a017

[52] Tabi T, Sajo IE, Szabo F et al (2010) Crystalline structure of annealed polylactic acid and its relation to processing. Express Polym Lett 4:659–668. https://doi.org/10.3144/expresspolymlett.2010.80

[53] Tábi T, Hajba S, Kovács JG (2016) Effect of crystalline forms (α′ and α) of poly(lactic acid) on its mechanical, thermo-mechanical, heat deflection temperature and creep properties. Eur Polym J 82:232–243. https://doi.org/10.1016/j.eurpolymj.2016.07.024

[54] Farid T, Herrera VN, Kristiina O (2018) Investigation of crystalline structure of plasticized poly (lactic acid)/Banana nanofibers composites. IOP Conf Ser Mater Sci Eng 369:012031. https://doi.org/10.1088/1757-899X/369/1/012031

[55] Baptista C, Azagury A, Shin H et al (2020) The effect of temperature and pressure on polycaprolactone morphology. Polymer 191:122227. https://doi.org/10.1016/j.polymer.2020.122227

[56] Hu W (2018) The physics of polymer chain-folding. Phys Rep 747:1–50. https://doi.org/10.1016/j.physrep.2018.04.004